Physics of the Earth and Planetary Interiors 290 (2019) 99–106

Contents lists available at ScienceDirect

Physics of the Earth and Planetary Interiors

journal homepage: www.elsevier.com/locate/pepi

Scaling behavior and source mechanism of tremor recorded at Erebus volcano, Ross island, Antarctica

K.I. Konstantinou*, M. Astrid Ardiani, M.R.P. Sudibyo[1]

Department of Earth Sciences, National Central University, Jhongli, 320, Taiwan

ARTICLE INFO

Keywords:
Erebus
Tremor
Volcano
Scaling
Antarctica

ABSTRACT

Erebus is an intraplate stratovolcano of phonolitic composition located at the southern end of Terror Rift within the West Antarctica Rift system. The volcanic edifice of Erebus exhibits a summit plateau that hosts the main crater and a smaller inner crater that contains a persistent lava lake. Volcano-seismic signals are recorded at Erebus by a permanent network of short-period and broadband seismometers installed around the volcano edifice. We investigate the duration-amplitude scaling of tremor recorded by the closest (~0.6–2 km) broadband stations to the inner crater during May 2002–April 2004 in order to elucidate the physical processes taking place at its source. After screening the data for signals related to non-volcanic sources such as iceberg calving, we obtained 72 tremor events. Spectral analysis reveals that these events were either harmonic exhibiting several overtones or broadband, but there were also mixed events that contained both of these two states. All tremor episodes considered in this study follow an exponential duration-amplitude distribution that implies a scale-bound source process. This precludes the possibility that any of these signals is related to iceberg calving near Ross island, or that rock fracturing processes play any role in tremor generation. The large viscosity of phonolitic magma (~$10^{5.3}$ Pa s) suggests that source mechanisms which require high flow speeds in order to excite tremor are unlikely to operate at Erebus. On the other hand, oscillations of CO_2 bubble clouds formed at localized asperities within the magma chamber represent a scale-bound source that is also consistent with the observed oxidation state of ascending gas and with the deep (~5–7 km) location of the tremor source. These results are important for understanding tremor processes at volcanoes which, similar to Erebus, exhibit vigorous convection in their shallow plumbing system.

1. Introduction

Scaling relationships between the number and size of geophysical phenomena have been extensively developed and studied in the literature as a means of understanding the source process of these phenomena (e.g., Simkin, 1993; Krumbholz et al., 2014; Papale, 2018). Power and exponential law are two of the simplest models that have been fitted to these relationships, each of them signifying a physically distinct source process. Power law models are related to scale invariant processes where there is no characteristic length scale involved, as exemplified by the frequency-magnitude scaling of earthquakes (Gutenberg and Richter, 1954). Exponential law models represent scale-bound processes that are described by values distributed around a characteristic length scale, as for example seamount heights (Smith and Jordan, 1987). Volcanic tremor is a continuous signal with variable duration that is usually recorded near active volcanoes before, during and after eruptions (Konstantinou and Schlindwein, 2003). Signals similar to volcanic tremor can be also observed in large hydrothermal systems and are attributed to fluid-solid interaction (see for example De Lauro et al., 2012, 2013; Capuano et al., 2016). Unlike earthquakes, scaling relationships for tremor have been developed by substituting frequency of occurrence with signal duration and magnitude with seismic amplitude. Duration-amplitude distributions of tremor at different volcanoes worldwide have been found to consistently follow the exponential law model (Benoit et al., 2003; DeRoin et al., 2015; Arámbula-Mendoza et al., 2016), therefore the tremor source process is characterized by a mean length scale that may correspond for example to a conduit filled with fluid. However, sudden changes in tremor scaling behavior from exponential to power law have also been documented (Sandanbata et al., 2015) and may represent the influence of rock failure processes on the tremor source.

Erebus is an intraplate stratovolcano (~3794 m high) of phonolitic

* Corresponding author.
E-mail address: kkonst@ncu.edu.tw (K.I. Konstantinou).
[1] Now at: *Geophysical Engineering Program, Institut Teknologi Sumatera, South Lampung, Indonesia.*

https://doi.org/10.1016/j.pepi.2019.03.010
Received 22 November 2018; Received in revised form 18 February 2019; Accepted 27 March 2019
Available online 03 April 2019
0031-9201/

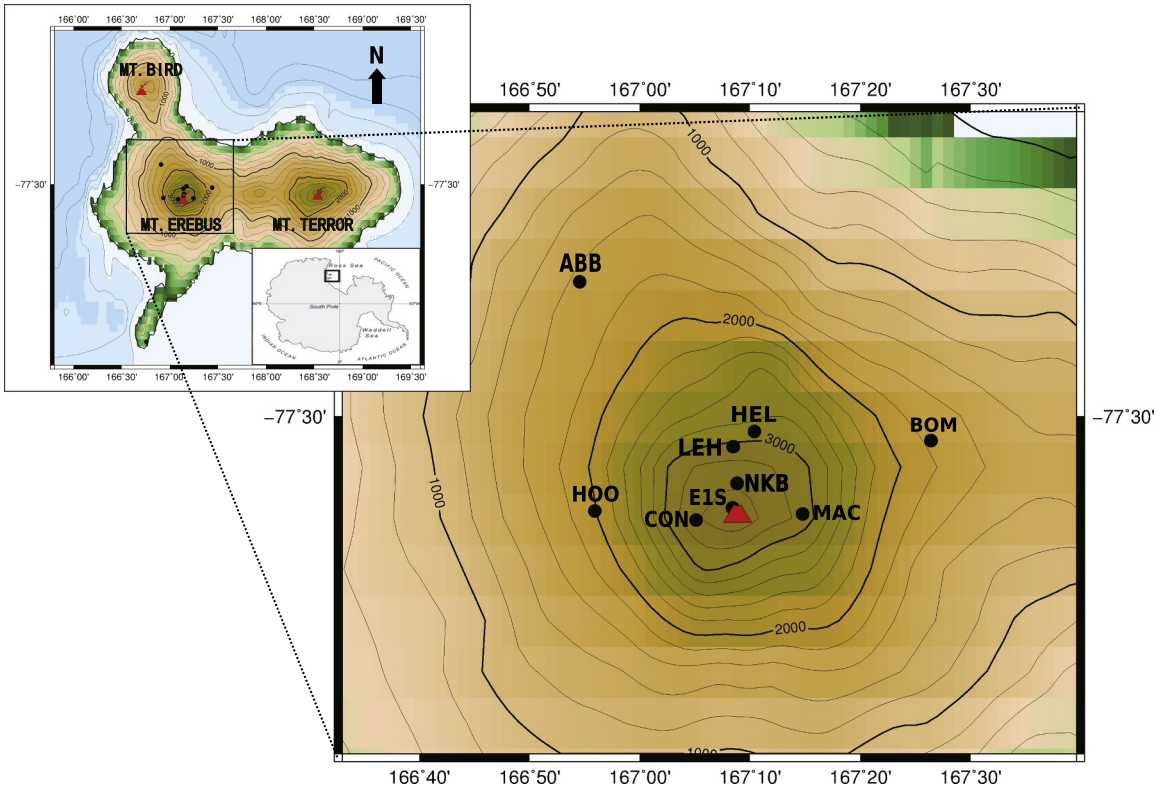

Fig. 1. Topographic map showing the Erebus volcano edifice and the location of seismic stations as black dots. The red triangle symbolizes the location of the lava lake. The larger inset shows a topographic map of Ross island and its three highest picks (Mt. Bird, Mt. Erebus, Mt. Terror) as red triangles. The smaller inset shows the location of Ross island as a black square relative to the continent of Antarctica. (For interpretation of the references to colour in this figure legend, the reader is referred to the web version of this article.)

composition that is located at the southern end of Terror Rift within the West Antarctica Rift system (Kyle et al., 1992; Behrendt, 1999) (Fig. 1). Volcanism there is a consequence of crustal rifting on top of a mantle plume, as evidenced by tomographic images that show a low velocity anomaly extending down to 400 km within the mantle (Gupta et al., 2009). The volcanic edifice of Erebus exhibits a summit plateau that hosts the main crater with a diameter of 600 m. A smaller inner crater with 200 m diameter exists within the main crater, containing a persistent lava lake. The seismic activity at Erebus is monitored by a permanent network of single-component 1 Hz seismometers and three-component broadband sensors installed by the New Mexico Institute of Mining and Technology (cf. Fig. 1). The majority of volcano-seismic signals recorded at Erebus consists of Strombolian explosions as well as very-long-period signals generated by volumetric changes of decompressed gas slugs as they ascend through the feeding conduit towards the surface of the lava lake (Rowe et al., 1998, 2000; Dibble et al., 2008; De Lauro et al., 2009). Volcanic tremor was rarely observed at Erebus prior to 2000, with these few episodes exhibiting either monochromatic or harmonic spectral properties (Rowe et al., 2000). After this period tremor signals started occurring more often, exhibiting also sudden transitions from harmonic to broadband tremor and vice versa. Romero (2004) analyzed tremor activity at Erebus between June 2000 and July 2003 and identified hundreds of such episodes. The author selected 24 of these and located them by using three different techniques (amplitude distribution, semblance, cross-correlation of envelopes). All of the selected episodes were located beneath the Erebus summit or its flanks at depths 5–7 km. Such deep tremor source is in agreement with the fact that there is little correlation between tremor activity and the Strombolian explosions that take place near the surface of the lava lake.

In this work, we study the duration-amplitude distribution of tremor events that were recorded at Erebus from May 2002 until April 2004. The main issues that we wish to address by our analysis are: (1) the possible existence of transitions from exponential to power law behavior; and (2) which is the most plausible source mechanism of tremor that can fit our observations and the characteristics of the plumbing system beneath Erebus. First, we give an overview of the available data and describe the methodology utilized for the calculation of duration-amplitude distributions and the fitting with power/exponential law. Potential tremor generation models are then discussed in the context of the plumbing system beneath Erebus. Finally, we show that while previously proposed tremor models are unlikely to operate at Erebus, oscillations of bubble clouds forming inside the shallow magma chamber is a plausible source for tremor generation.

2. Data characteristics and selection

For the needs of this study we focused on the period starting from mid-May 2002 until late April 2004 when according to Romero (2004) there was significant tremor activity. We utilized data recorded by stations E1S and CON (cf. Fig. 1) which are equipped with a broadband three-component sensor recording at a sampling rate of 100 samples/s. E1S is the closest (~0.69 km) station to the lava lake and operated continuously from May 2002 until May 2003, during November 2003, and from January until April 2004. During the period from June to October 2003 as well as December 2003, when data from E1S was not available, we performed the analysis using data recorded by station CON that was located about 2 km away from the lava lake. By performing a visual inspection of the recorded data it was possible to identify a total of 278 tremor episodes. In order to properly classify the different tremor events based on their spectral properties, we calculated spectrograms for each of them by using the Short-Time Fourier Transform (STFT) for a 10 s sliding window with 50% overlap after applying a Hanning tapering function at each window. In this way we are able to identify three groups: (1) harmonic events containing a fundamental

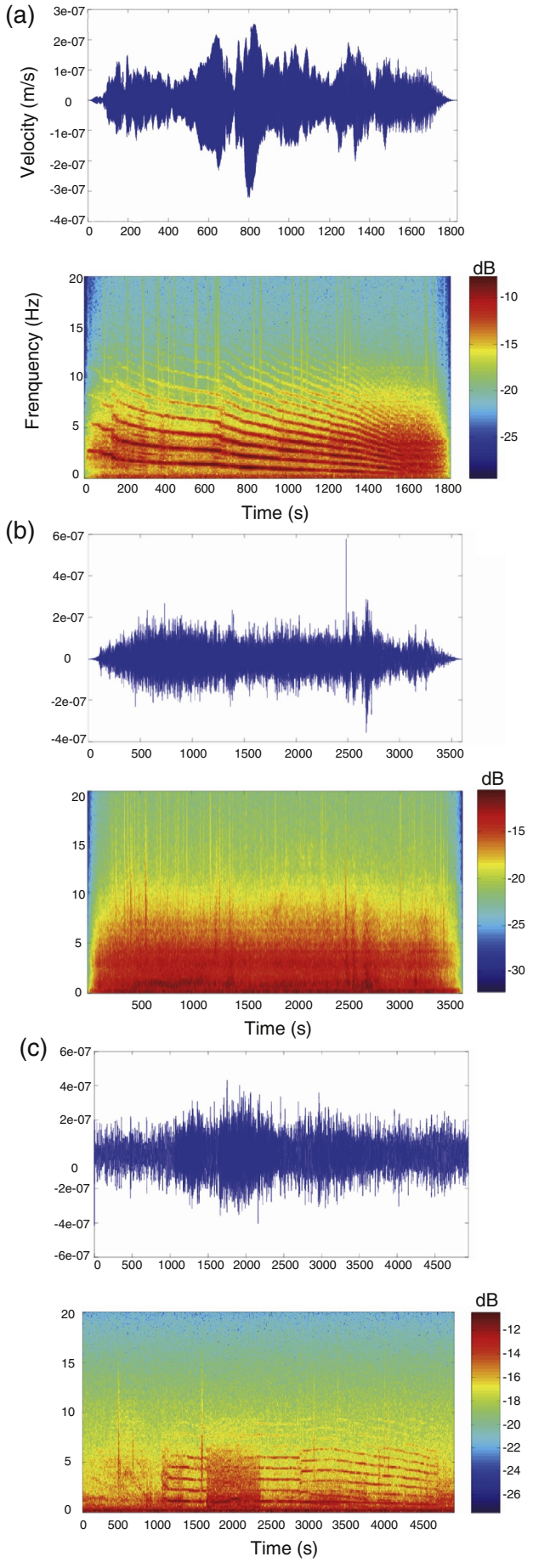

Fig. 2. Vertical component velocity waveforms and corresponding spectrograms for (a) harmonic tremor with gliding recorded on 17 May 2002 at 19:43:42, (b) broadband tremor recorded on 28 May 2002 at 01:04:48, and (c) mixed tremor episode recorded on 1 April 2003 at 09:34:32. All times refer to UTC time frame.

frequency and higher overtones, (2) broadband events where no specific spectral peaks could be observed, and (3) events that started as harmonic but switched to broadband and back to harmonic (hereafter called mixed tremor). In tremor events that contain higher overtones, a common feature is the presence of gliding where the overtone frequencies may steadily increase ("gliding-up") or decrease ("gliding-down") in unison. Fig. 2 shows waveforms and spectrograms of one representative example from each of these groups. We subsequently deconvolved the instrument response and bandpass filtered the vertical component waveforms of each tremor event between 0.5 and 15 Hz in order to remove microseismic and higher frequency noise. We then calculated the envelopes of displacement waveforms and converted them to reduced displacement D_R which is a normalized amplitude metric for volcanic tremor (Aki and Koyanagi, 1981). As mentioned earlier, tremor at Erebus likely has a deep source of several km below the main crater, therefore it is reasonable to assume that the tremor wavefield consists mostly of body waves. In this case $D_R = (A/2\sqrt{2}) \times (r/M)$, where A is the tremor amplitude, r is the distance of the station from the lava lake (i.e. the tremor source depth is not taken into account) and M is the sensor magnification given by Romero (2004).

Except from seismic signals related to volcanic activity, the network around Erebus also records signals generated by activities such as iceberg breakup and drifting. Talandier et al. (2002) were the first to observe such signals recorded by seismic stations in French Polynesia during late 2000. The authors attributed them to icebergs calving off the Ross Ice Self and subsequently drifting in the Ross Sea. More importantly, these signals appeared to be very similar to volcanic tremor exhibiting frequencies up to 7 Hz and in many cases several overtones were also present. Romero (2004) investigated whether any of these iceberg tremor signals were recorded by the Erebus seismic network. This search showed that out of 13 tremor events reported by Talandier et al. (2002) only 4 of them were actually recorded by stations at Erebus. In a later study, Martin et al. (2010) analyzed a long-lasting tremor signal generated by iceberg breakup at Cape Adare (NW of Erebus) and compared its spectral characteristics across stations whose distance ranged from 0.7° to 17.9°. These stations also included station CON (at a distance 5.6°) that recorded the iceberg tremor as a low-frequency (< 2 Hz), low-amplitude signal. Compared to other stations that were more distant than CON from the iceberg source, the signal recorded at CON appeared depleted in higher frequency energy. This observation can be easily explained by considering the high levels of intrinsic and scattering attenuation beneath Erebus (Zandomeneghi et al., 2013). In order to avoid the inclusion in our dataset of iceberg tremor, we screened the initial 278 events by selecting a subset of 72 events with significant energy above 4 Hz and mean reduced displacement of 5 cm^2 or higher. One could argue that these selection criteria may be adequate to exclude far-field iceberg tremor but not iceberg signals that originate close to Ross island. Kirkham et al. (2017) investigated the scaling behavior of iceberg tremor signals that are produced during glacier calving and during the disintegration of icebergs when they are drifting in the open ocean. The authors showed that while seismic signals due to iceberg disintegration follow a log-normal scaling law, signals generated by iceberg breakup near the calving front exhibit power law behavior. In this sense we would expect that if iceberg tremor occurs near Ross island, it will be associated with iceberg breakup near the calving front of the Ross Ice Self and will follow a power law scaling. On this basis, the analysis of duration-amplitude scaling described in the next section will be able to detect any power law behavior if it exists in our data.

3. Duration-amplitude scaling

In order to analyze the duration-amplitude scaling of each tremor event the onset and end times of each tremor episode were estimated by considering a lowest threshold value of D_R ranging from 3 to 5 cm^2 even though we found that the fitting results were not significantly different. Cumulative duration in seconds was then calculated for a set of different reduced displacement values as shown in the example of Fig. 3. Following Benoit et al. (2003) we fit to the duration-amplitude distribution of each tremor episode first an exponential law of the form

$$d(D_R) = d_t e^{-\lambda D R} \quad (1)$$

where D_R is the tremor amplitude, d is the duration of tremor with amplitudes larger than D_R, d_t is the total duration of the tremor episode and λ is the slope of the line. The inverse of the slope λ^{-1} can be considered as the mean or characteristic amplitude of the distribution and can also be taken as proportional to the geometric dimension of the tremor source. The power law that we fitted to each distribution has the form of

$$d(D_R) = d_t (D_R)^{-\gamma} \quad (2)$$

where γ is the slope of the power law line. We evaluated the goodness-of-fit for each of these models by calculating the correlation coefficient (R^2) and also by performing a chi-square (χ^2) test in a similar way as Benoit et al. (2003). It should be noted that the main function of the χ^2-test is to give statistical bounds of how likely it is for a particular model to fit the observations, rather than unambiguously accept or reject any given model. For all 72 selected tremor events we find that they can be fitted better with an exponential rather than a power law, as attested by the high values of the correlation coefficient and the χ^2-test using a confidence level of 95% (Fig. 4). This precludes the possibility that any of these signals are related to iceberg calving near Ross island, or that

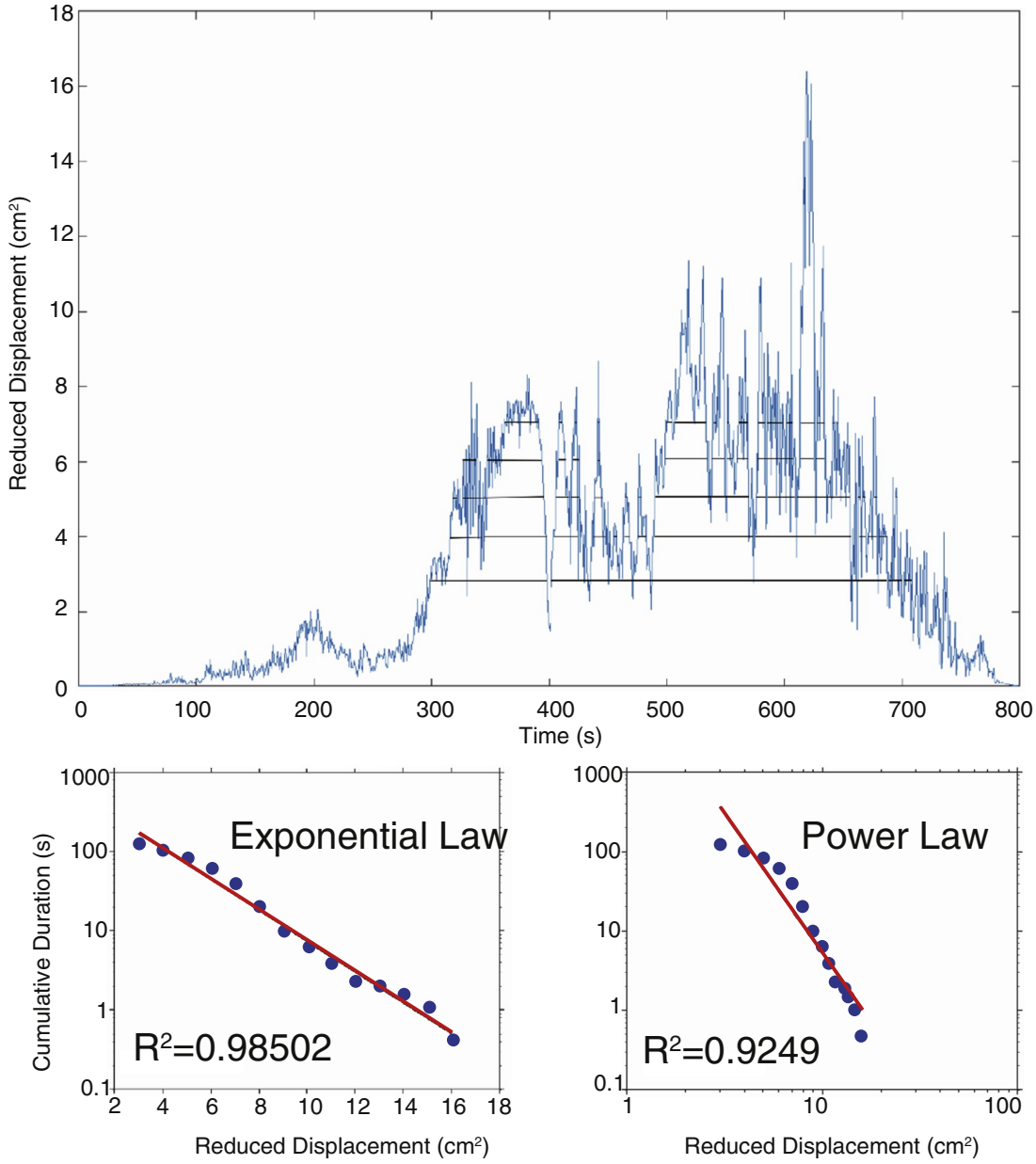

Fig. 3. Example of the calculation of duration-amplitude distribution for a tremor event and fitting of the values with exponential and power law. Black horizontal lines indicate cumulative duration for particular values of reduced displacement. Red lines represent the best fit line in a least-squares sense. R^2 represents the correlation coefficient between cumulative duration and reduced displacement. (For interpretation of the references to colour in this figure legend, the reader is referred to the web version of this article.)

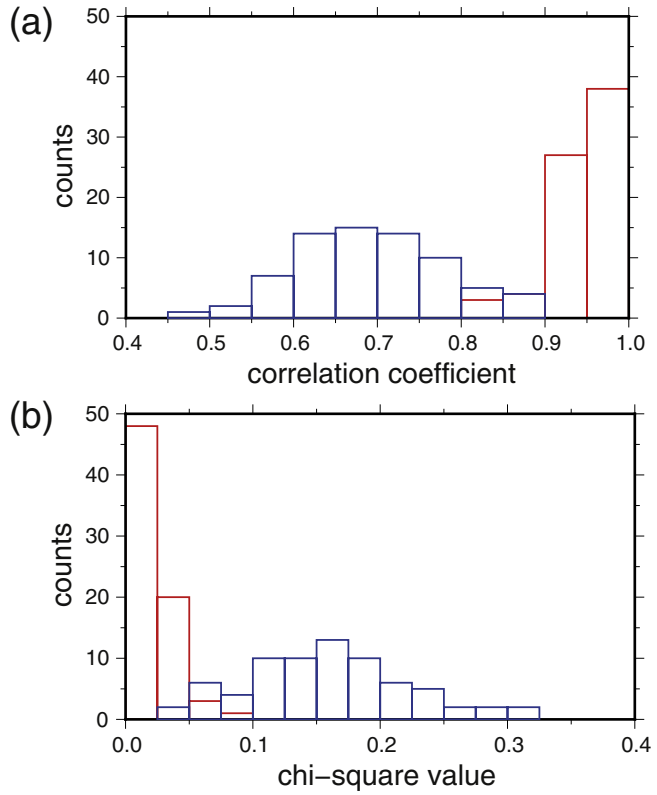

Fig. 4. Histograms showing the distribution of (a) the correlation coefficient (R^2), and (b) chi-square values after fitting the duration-amplitude data with the different scaling models. Red bars represent the results for exponential law, while blue bars correspond to the results for power law. (For interpretation of the references to colour in this figure legend, the reader is referred to the web version of this article.)

rock fracturing processes may be operating at the tremor source. It also implies that if the tremor source is scale-bound, then the characteristic amplitude (i.e. λ^{-1}) of each event should be inversely proportional to its observed lowest frequency. Fig. 5 shows this kind of relationship, where almost all of the studied tremor events attain increasing characteristic amplitudes as their lowest frequency decreases. The catalog of the tremor events analyzed, as well as information about the fitting parameters (d_t, λ, γ) and about R^2 and χ^2-test can be found in Table S1 of the supplementary material that accompanies this work.

4. Source mechanism of tremor

4.1. Plumbing system and potential tremor models

Current knowledge about the plumbing system beneath Erebus comes mostly from studies of gas emissions and petrological analysis of bombs ejected during Strombolian eruptions. In particular, the magmatic system consists of three parts: a deep mantle reservoir; a shallow magma chamber; and the lava lake in the inner crater (Fig. 6). The deep mantle reservoir contains basanite and acts as the primary source of melt and CO_2 which is the main gas phase exsolved (Oppenheimer et al., 2009, 2011). The constant levels of lava in the lake and the lack of any edifice deformation preclude the occurrence of frequent injections of basanite into the shallow magma chamber and point to a constriction in the conduit that connects the two reservoirs (Oppenheimer et al., 2011). This has as a consequence that melt can go through only episodically, while large quantities of CO_2 can pass and ascend towards the lava lake as decompressed slugs. The shallow reservoir extends from 7.5 km to 4 km as suggested by the mineral assemblage of ejected bombs (Moussallam et al., 2013). It is connected

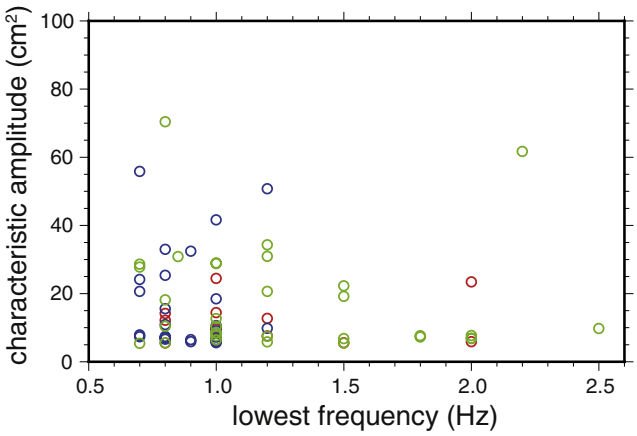

Fig. 5. Diagram of the variation of characteristic amplitude (in cm^2) of each tremor event as a function of its lowest signal frequency. Red circles represent harmonic events, blue circles are broadband ones and green circles are mixed tremor events. (For interpretation of the references to colour in this figure legend, the reader is referred to the web version of this article.)

with the lava lake through a conduit where bi-directional flow may occur, in the sense that gas-rich melt ascends in the central part of the conduit, while degassed magma flows downwards along its periphery. This bi-directional flow is responsible for the vigorous convection observed in the lava lake and in the shallow magma chamber, as inferred from textural analysis of anorthoclase feldspar megacrystals (Moussallam et al., 2015).

The tremor source at Erebus is located within the same depth range as the shallow magma chamber (~5–7 km) and the duration-amplitude analysis suggests that it exhibits a characteristic length scale. It is also capable of generating harmonic and broadband signals or display sudden transitions from harmonic to broadband and vice versa. The mechanism of nonlinear excitation by fluid flow proposed by Julian (1994) could explain these sudden transitions and would operate at places within the plumbing system of Erebus where constrictions exist. However, this model has been built on the assumption that the fluid is basaltic melt with viscosity 500 Pa s that can flow fast enough so as to excite oscillations of the conduit walls (see Rust et al., 2008). The bulk viscosity of phonolitic magma at Erebus has been estimated to be $10^{5.3}$ Pa s, even though it may be 0.5–1.5 log units lower if the effect of dissolved volatiles in the form of bubbles is taken into account (Le Losq et al., 2015). In either way such viscosity is several times larger than what is assumed in Julian's model and makes high flow speeds difficult to attain. An alternative model for tremor generation would be eddy shedding (Hellweg, 2000), where vortices are created as fluid flows past a geometrical obstacle and these vortices exert a variable force on the conduit walls that in turn generates seismic waves. For this mechanism to excite tremor with a fundamental frequency close to 0.7 Hz through an obstacle with a linear dimension between 10 and 100 m, the flow velocity must be in the order of several tens of meters per second (see Fig. 4 in Hellweg, 2000). This condition is again unlikely to be satisfied within the shallow magma chamber given the high viscosity of the phonolitic melt.

Oscillations of bubble clouds have been previously suggested as a potential mechanism for tremor generation at Kilauea volcano, Hawaii, which also hosts a permanent lava lake (Matoza et al., 2010; Unglert and Jellinek, 2015). In such a mechanism geometrical irregularities in the walls of the shallow magma chamber may act as sites where ascending bubbles of CO_2 concentrate and form clouds. Oscillations of such clouds with harmonic or broadband signatures can be generated depending on the arrangement of the bubbles, the variations in their radii and on the degree of heterogeneity of the pressure and flow field. Bubble cloud oscillation represents a source with a characteristic length scale determined by the geometrical irregularities of the plumbing

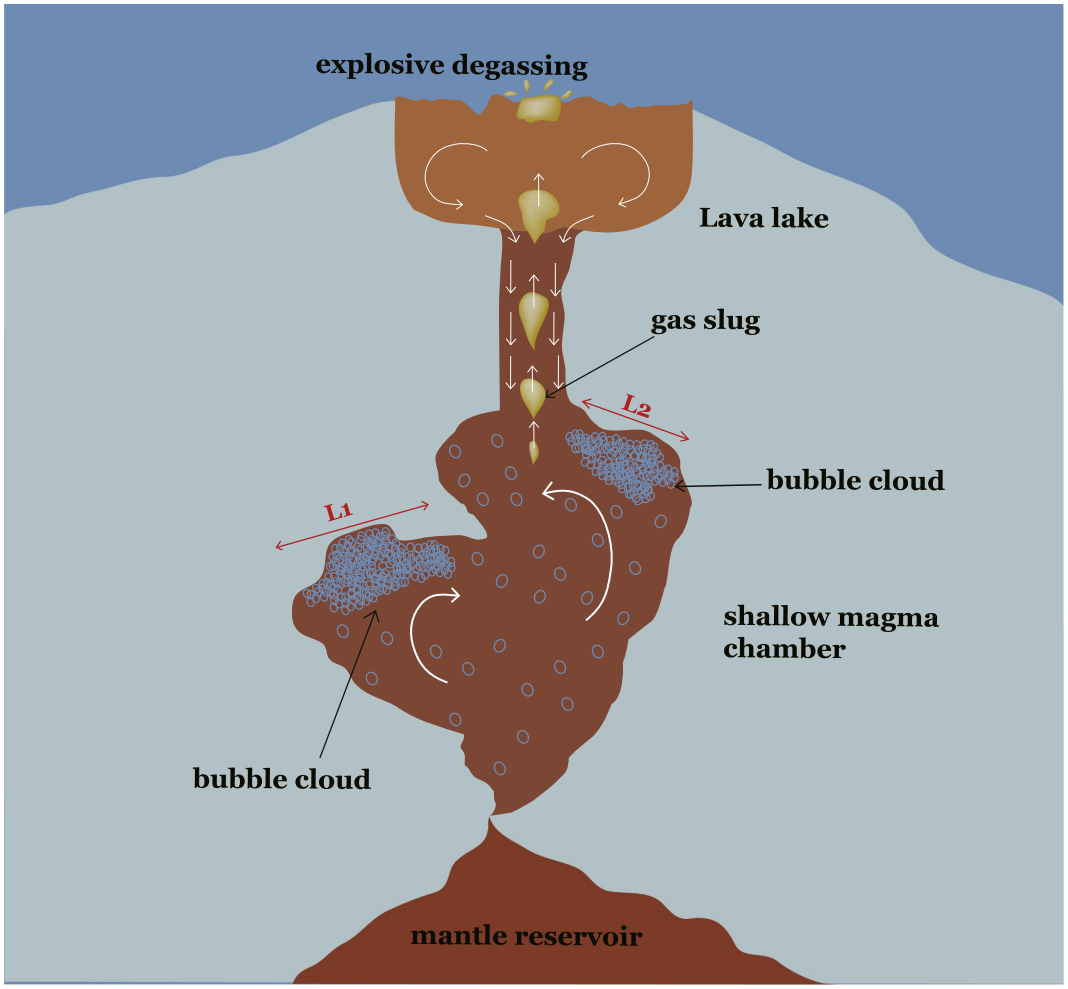

Fig. 6. Cartoon illustrating the geometric configuration of the plumbing system beneath Erebus based on available information (see text for more details). Straight arrows indicate the movement of the gas/melt, while curved arrows indicate convection. Bubble clouds may form at geometrical irregularities of the magma chamber walls and oscillate as a result of different pressure and flow fields. The characteristic length scale of the clouds (L_1 and L_2) is then determined by the geometry of the irregularity itself.

system near which the bubbles tend to accumulate (cf. Fig. 6), and hence may produce different populations of tremor characteristic amplitudes. This mechanism is also consistent with the observation that the ascending gas slugs at Erebus are more oxidized than the lava lake itself, which can be explained only if gas first accumulates near asperities of the plumbing system before ascending to the surface episodically (Moussallam et al., 2014). In the next section we examine whether the necessary conditions for bubble cloud resonance at Erebus are fulfilled.

4.2. Conditions for bubble cloud resonance

Resonance of a bubble cloud can occur on condition that the resonance frequencies lie within the range of τ_g^{-1} and τ_b^{-1} (Ichihara and Kameda, 2004), where τ_g is the characteristic time of volatile transfer into and out of the bubbles by diffusion, while τ_b is the characteristic time of bubble expansion which primarily depends on melt viscosity. Ichihara and Kameda (2004) have defined the characteristic time of mass transfer into and out of the bubbles by diffusion of volatiles as

$$\tau_g = 2\pi R^2/9\kappa_{gl}\,(\rho_m P_0/\rho_g \cdot \partial C_{eq}/\partial P)^{-2} \quad (3)$$

where R is the radius of the bubbles, κ_{gl} is diffusivity of the volatile in the liquid, ρ_m is density of the melt, P_0 is the magmastatic pressure, ρ_g is density of the gas and $C_{eq}(P)$ is volatile concentration that is in equilibrium with the gas phase at pressure P. We assume the bubble radius R to be 1 mm, while we calculate diffusivity κ_{gl} of CO_2 using the equation (Dobran, 2001)

$$\kappa_{gl} = 6.2 \times 10^{-4}\ \exp(-144{,}600/R_g T) \quad (4)$$

where R_g is the gas constant equal to 8.31 J K^{-1} mol^{-1} and T is temperature which for Erebus magma is 1288 K (Le Losq et al., 2015). Substituting these values to Eq. (4) will give $\kappa_{gl} = 4.1 \times 10^{-10}$ m^2/s. The density of the Erebus melt is taken as 2433 kg/m^3 (Le Losq et al., 2015) and then the magmastatic pressure can be easily calculated as $P_0 = \rho_m g z$, where g is acceleration of gravity and z is depth. For depth values of 5 km and 7 km consistent with tremor source depths the magmastatic pressure varies from 119 MPa to 167 MPa respectively. At these depths and temperature we consider CO_2 to be a supercritical fluid with density of 387 kg/m^3. The solubility of CO_2 for various types of magma is given by $C_{eq}(P) = 4.4 \times 10^{-12} \times P$ (Dobran, 2001). Substituting these values to Eq. (3) will give $\tau_g = 7.6 \times 10^7$ s for a depth of 5 km and 3.8×10^7 s for a depth of 7 km. The corresponding frequencies are 1.3×10^{-8} Hz and 2.5×10^{-8} Hz that are much lower than the lowest frequency (~0.7 Hz) that we can observe.

On the other hand, the characteristic time of bubble volume relaxation τ_b is given by the equation (Ichihara and Kameda, 2004).

$$\tau_b = 8\pi\eta/3\gamma_g P_0 \quad (5)$$

where η is the viscosity of the melt and γ_g is the ratio of specific heats of the gas phase. We assume an average viscosity of $10^{5.3}$ Pa s for the

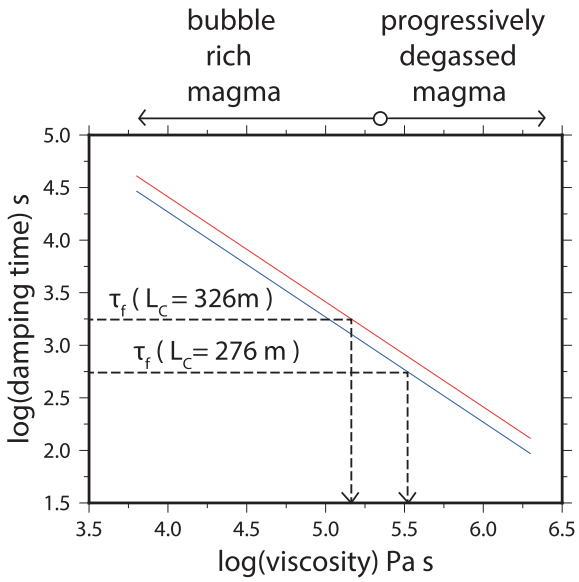

Fig. 7. Diagram showing the relationship between damping time of bubble cloud oscillations and melt viscosity. Red line corresponds to a characteristic length of 326 m and the blue one to 276 m. The dashed lines connect the forcing time value for each characteristic length with the corresponding viscosity below which the damping time is always larger than the forcing time. Values of viscosity higher than the average ($10^{5.3}$ Pa s) represent progressively degassed magma, while values lower than this correspond to magma with a higher fraction of bubbles. (For interpretation of the references to colour in this figure legend, the reader is referred to the web version of this article.)

magma at Erebus (Le Losq et al., 2015) while we take $\gamma_g = 1.28$ for CO_2. Then for a magmastatic pressure of 119 MPa (depth of 5 km) $\tau_b = 0.0109$ s and for 167 MPa (depth of 7 km) $\tau_b = 0.0078$ s. This implies frequencies that range from about 91 Hz up to 128 Hz. Even if we increase the viscosity to the value consistent with degassed magma ($\sim 10^{6.3}$ Pa s), inferred by Le Losq et al. (2015), we obtain frequencies of 9 Hz and 13 Hz respectively that are close to the highest frequencies observed in our dataset. We conclude therefore that resonance of bubble clouds is a plausible mechanism for tremor generation at Erebus for the full range of magma viscosity values.

4.3. Timescales of oscillation forcing and damping

Another issue that has to be considered is whether the viscosity of phonolitic magma is so high that may damp the oscillations of the bubble cloud very quickly without allowing long duration tremor to be generated. In order to investigate this, in what follows we calculate the range of potential values of the forcing and damping timescales of bubble cloud oscillations. The characteristic frequency f_c of the bubble cloud oscillations is connected to the physical properties of the melt and the characteristic length of the source L_c by the relationship (Unglert and Jellinek, 2015).

$$f_c = 1/2\pi\,(3P_0/\phi\rho_m L_c^2)^{1/2} \quad (6)$$

where ϕ is the average porosity of the bubble cloud. Assuming that $\phi = 0.1$ and for magmastatic pressures at 5 and 7 km, the characteristic length corresponding to $f_c = 0.7$ Hz is in the range of 276–326 m respectively. Higher values of average porosity will produce a progressively less continuous cloud mixture and will increase significantly the viscosity of the magma (e.g. Gonnermann and Manga, 2007). Based on the plumbing system configuration beneath Erebus described previously, the bubble cloud is most likely forced into resonance by vertical and lateral flow of melt controlled by the geometrical irregularities of the shallow magma chamber. The timescale τ_f of this forcing can be approximated as L_c/V_m where V_m is the flow speed of magma. The flow speed is likely quite small, in the order of 0.1 m/s if we consider the measured speed of the lava lake surface (Oppenheimer et al., 2009). For the values of L_c calculated above we obtain $\tau_f = 2758$–3263 s that should be smaller than the time needed for the oscillations to be damped. The time that the bubble cloud oscillation needs in order to get damped can be approximated by the relationship (Unglert and Jellinek, 2015).

$$\tau_d = \rho_m L_c^2/\eta \quad (7)$$

Fig. 7 shows the falloff of damping time for the two characteristic lengths as a function of melt viscosity within the range of values appropriate for Erebus. It can be seen that for viscosity lower than $10^{5.5}$ and $10^{5.2}$ Pa s the value of τ_d is larger than the forcing time for the two characteristic lengths. This means that magma that is rich in bubbles will tend to have lower viscosity (Pistone et al., 2013; Le Losq et al., 2015) and therefore will produce damping times that are longer than the corresponding forcing times.

5. Conclusions

We analyzed 72 tremor events recorded from May 2002 until April 2004 in order to understand their spectral properties and the scaling behavior of their duration-amplitude distribution. Based on their frequency content these events were grouped into three categories, namely harmonic, broadband or a mixture of these two states, with observed frequencies between 0.7 and 13 Hz. The duration-amplitude distribution of all tremor events analyzed follows an exponential law which suggests that the tremor source exhibits some characteristic length scale. This casts doubt on the hypothesis that these signals are generated by a fracture-related process such as iceberg calving, or by a destructive source that requires rock fracturing within the Erebus plumbing system. Previously proposed tremor source models require high flow speed for magma (> 1 m/s) in order to excite different oscillation mechanisms, a condition which is unlikely to be fulfilled at Erebus due to the relatively high viscosity of its melt. On the other hand, oscillations of CO_2 bubble clouds is a plausible mechanism for tremor generation at Erebus for two reasons: first, it is consistent with observations which require that before ascending to the surface as a slug, gas accumulates near localized asperities within the plumbing system; and second, fixed geometrical properties of these asperities may give rise to scale-bound sources. Such a source mechanism has been already invoked in order to explain tremor observed at Kilauea volcano, Hawaii, which shares common characteristics with Erebus in terms of a geometrically complex plumbing system and the existence of a permanent lava lake. Thus far bubble cloud oscillations have received much less attention compared to other potential tremor sources, even though such a mechanism may be important in volcanoes that exhibit vigorous convection in their shallow plumbing system. Future studies should therefore focus on better understanding this tremor source by performing numerical and/or analog modeling under different flow and boundary conditions.

Supplementary data to this article can be found online at https://doi.org/10.1016/j.pepi.2019.03.010.

Acknowledgments

This work was funded by grant MOST-106-2116-M-008-007 awarded to the first author by the Ministry of Science and Technology, Taiwan. M. A. Ardiani and M. R. P. Sudibyo held a postgraduate scholarship from the School of Earth Sciences at National Central University. The continuous waveform data used in this study is freely available from IRIS. We would like to thank three anonymous reviewers and the Editor Mark Jellinek for their helpful comments that improved the clarity of this paper.

References

Aki, K., Koyanagi, R.Y., 1981. Deep volcanic tremor and magma ascent mechanism under Kilauea, Hawaii. J. Geophys. Res. 86, 7095–7109.

Arámbula-Mendoza, R., Valdes-Gonzalez, C., Varley, N., Reyes-Pimentel, T.A., Juarez-Garcia, B., 2016. Tremor and its duration-amplitude distribution at Popocatepetl volcano, Mexico. Geophys. Res. Lett. 43, 8994–9001. https://doi.org/10.1002/2016GL070227.

Behrendt, J., 1999. Crustal and lithospheric structure of the West Antarctica Rift System from geophysical investigation: a review. Glob. Planet. Chang. 23, 24–44.

Benoit, J.P., McNutt, S.R., Barboza, V., 2003. Duration-amplitude distribution of volcanic tremor. J. Geophys. Res. 108 (3), 2146. https://doi.org/10.1029/2001JB001520.

Capuano, P., De Lauro, E., De Martino, S., Falanga, M., 2016. Detailed investigation of long-period activity at Campi Flegrei by convolutive independent component analysis. Phys. Earth Planet. Inter. 253, 48–57. https://doi.org/10.1016/j.pepi.2016.02.003.

De Lauro, E., De Martino, S., Falanga, M., Palo, M., 2009. Modeling the macroscopic behavior of Strombolian explosions at Erebus volcano. Phys. Earth Planet. Inter. 176, 174–186. https://doi.org/10.016/j.pepi.2009.05.003.

De Lauro, E., Falanga, M., Petrosino, S., 2012. Study on the long-period source mechanism at Campi Flegrei (Italy) by a multi-parametric analysis. Phys. Earth Planet. Inter. 206–207, 16–30. https://doi.org/10.1016/j.pepi.2012.06.006.

De Lauro, E., De Martino, S., Falanga, M., 2013. Synchronization between tides and sustained oscillations of the hydrothermal system of Campi Flegrei (Italy). Geochem. Geophys. Geosyst. 14 (8), 2628–2637. https://doi.org/10.1002/ggge.20149.

DeRoin, N., McNutt, S.R., Thompson, G., 2015. Duration-amplitude relationships of volcanic tremor and earthquake swarms preceding and during the 2009 eruption of Redoubt volcano, Alaska. J. Volcanol. Geotherm. Res. 292, 56–69. https://doi.org/10.1016/j.volgeores.2015.01.003.

Dibble, R.R., Kyle, P.R., Rowe, C.A., 2008. Video and seismic observations of Strombolian eruptions at Erebus volcano, Antarctica. J. Volcanol. Geotherm. Res. 177, 619–634. https://doi.org/10.1016/j.volgeores.2008.07.020.

Dobran, F., 2001. Volcanic Processes: Mechanisms in Material Transport. Kluwer Academic, New York.

Gonnermann, H., Manga, M., 2007. The fluid mechanics inside a volcano. Annu. Rev. Fluid Mech. 39, 321–356.

Gupta, S., Zhao, D., Rai, S.S., 2009. Seismic imaging of the upper mantle under the Erebus hotspot in Antarctica. Gondwana Res. 16, 109–118.

Gutenberg, B., Richter, C.F., 1954. Magnitude and energy of earthquakes. Ann. Geofis. 9, 1–15.

Hellweg, M., 2000. Physical models for the source of Lascar's harmonic tremor. J. Volcanol. Geotherm. Res. 101, 183–198.

Ichihara, M., Kameda, M., 2004. Propagation of acoustic waves in a visco-elastic two-phase system: influences of the liquid viscosity and the internal diffusion. J. Volcanol. Geotherm. Res. 137, 73–91. https://doi.org/10.1016/j.jvolgeores.2004.05.001.

Julian, B.R., 1994. Volcanic tremor: nonlinear excitation by fluid flow. J. Geophys. Res. 99, 11859–11877.

Kirkham, J.D., Rosser, N.J., Wainright, J., Vann Jones, E.C., Dunning, S.A., Lane, V.S., Hawthorne, D.E., Strzelecki, M.C., Szczuniski, W., 2017. Drift-dependent changes in iceberg size-frequency distributions. Sci. Rep. 7, 15991. https://doi.org/10.1038/s41598-017-14863-2.

Konstantinou, K.I., Schlindwein, V., 2003. Nature, wavefield properties and source mechanism of volcanic tremor: a review. J. Volcanol. Geotherm. Res. 119, 161–187.

Krumbholz, M., Hieronymous, C.F., Burchardt, S., Troll, V.R., Tanner, D.C., Friese, N., 2014. Weibull-distributed dyke thickness reflects probabilistic character of host-rock strength. Nat. Commun. 5, 3272. https://doi.org/10.1038/ncomms4272.

Kyle, P., Moore, J.A., Thirlwall, M.F., 1992. Petrologic evolution of anorthoclase phonolite lavas at Mt Erebus, Ross island, Antarctica. J. Petrol. 33, 849–875.

Le Losq, C., Neuville, D.R., Moretti, R., Kyle, P.R., Oppenheimer, C., 2015. Rheology of phonolitic magmas – the case of the Erebus lava lake. Earth Planet. Sci. Lett. 411, 53–61. https://doi.org/10.1016/j.epsl.2014.11.042.

Martin, S., Drucker, R., Aster, R., Davey, F., Okal, E., Scabos, T., MacAyal, D., 2010. Kinematic and seismic analysis of giant tabular iceberg breakup at Cape Adare, Antarctica. J. Geophys. Res. 115, B06311. https://doi.org/10.1029/2009JB006700.

Matoza, R.S., Fee, D., Garcés, M.A., 2010. Infrasonic tremor wavefield of the Pu'u O'o crater complex and lava tube system, Hawaii, in April 2007. J. Geophys. Res. 115, B12312. https://doi.org/10.1029/2009JB007192.

Moussallam, Y., Oppenheimer, C., Scaillet, B., Kyle, P.R., 2013. Experimental phase-equilibrium constraints on the phonolite magmatic system of Erebus volcano, Antarctica. J. Petrol. 54 (7), 1285–1307. https://doi.org/10.1093/petrology/egt012.

Moussallam, Y., Oppenheimer, C., Scaillet, B., Gaillard, F., Kyle, P., Peters, N., Hartley, M., Berlo, K., Donovan, A., 2014. Tracking the changing oxidation state of Erebus magmas, from mantle to surface, driven by magma ascent and degassing. Earth Planet. Sci. Lett. 393, 200–209. https://doi.org/10.1016/j.epsl.2014.02.055.

Moussallam, Y., Oppenheimer, C., Scaillet, B., Buisman, I., Kimball, C., Dunbar, N., Burgisser, A., Schipper, C.I., Andujar, J., Kyle, P., 2015. Megacrystals track magma convection between reservoir and surface. Earth Planet. Sci. Lett. 413, 1–12. https://doi.org/10.1016/j.epsl.2014.12.022.

Oppenheimer, C., Lomakina, A.S., Kyle, P.R., Kingsbury, N.G., Boichu, M., 2009. Pulsatory magma supply to a phonolite lava lake. Earth Planet. Sci. Lett. 284, 392–398. https://doi.org/10.1016/j.epsl.2009.04.043.

Oppenheimer, C., Moretti, R., Kyle, P.R., Eschenbacher, A., Lowenstern, J.B., Hervig, R.L., Dunbar, N.W., 2011. Mantle to surface degassing of alkalic magmas at Erebus volcano, Antarctica. Earth Planet. Sci. Lett. 306, 261–271. https://doi.org/10.1016/j.epsl.2011.04.005.

Papale, P., 2018. Global time-size distribution of volcanic eruptions on Earth. Sci. Rep. 8, 6838. https://doi.org/10.1038/s41598-018-25286.

Pistone, M., Caricchi, L., Ulmer, P., Reusser, E., Ardia, P., 2013. Rheology of volatile-bearing crystal mushes: mobilization vs. viscous death. Chem. Geol. 345, 16–39.

Romero, R.M., 2004. Analysis of tremor activity at Mt Erebus volcano, Antarctica (MS thesis). New Mexico Institute of Mining and Technology (141 pp.).

Rowe, C.A., Aster, R.C., Kyle, P.R., Schlue, J.W., Dibble, R.R., 1998. Broadband recording of Strombolian explosions and associated very-long-period seismic signals on Mt Erebus volcano, Ross island, Antarctica. Geophys. Res. Lett. 25 (13), 2297–2300.

Rowe, C.A., Aster, R.C., Kyle, P.R., Dibble, R.R., Schlue, J.W., 2000. Seismic and acoustic observations at Mt Erebus volcano, Ross island, Antarctica, 1994-1998. J. Volcanol. Geotherm. Res. 101, 105–128.

Rust, A.C., Balmforth, N.J., Mandre, S., 2008. The feasibility of generating low-frequency volcano seismicity by flow through a deformable channel. In: Lane, S., Gilbert, J.S. (Eds.), Fluid Motions in Volcanic Conduits: A Source of Seismic and Acoustic Signals. Geol. Soc. London, Special Publications 307. pp. 45–56. https://doi.org/10.1144/SP307.4.

Sandanbata, O., Obara, K., Maeda, T., Takagi, R., Satake, K., 2015. Sudden changes in the amplitude-frequency distribution of long-period tremors at Aso volcano, Southwest Japan. Geophys. Res. Lett. 42, 10,256–10,262. https://doi.org/10.1002/2015GL066443.

Simkin, T., 1993. Terrestrial volcanism in space and time. Annu. Rev. Earth Planet. Sci. 21, 427–452.

Smith, D.K., Jordan, T.H., 1987. The size distribution of Pacific seamounts. Geophys. Res. Lett. 14, 1119–1122.

Talandier, J., Hyvernaud, O., Okal, E.A., Piserchia, P.-F., 2002. Long-range detection of hydroacoustic signals from large icebergs in the Ross Sea, Antarctica. Earth Planet. Sci. Lett. 203, 519–534. https://doi.org/10.1016/S0012-821X(02)00867-1.

Unglert, K., Jellinek, A.M., 2015. Volcanic tremor and frequency gliding dike intrusions at Kilauea – a tale of three eruptions. J. Geophys. Res. Solid Earth 120. https://doi.org/10.1002/2014JB011596.

Zandomeneghi, D., Aster, R., Kyle, P., Barclay, A., Chaput, J., Knox, H., 2013. Internal structure of Erebus volcano, Antarctica imaged by high-resolution active-source seismic tomography and coda-interferometry. J. Geophys. Res. 118, 1–12. https://doi.org/10.1002/jgrb.50073.